JOURNAL OF GEOPHYSICAL RESEARCH, VOL. 91, NO. B11, PAGES 11,463–11,476, OCTOBER 10, 1986

Extensional Tectonics at The Geysers Geothermal Area, California

DAVID H. OPPENHEIMER

U.S. Geological Survey, Menlo Park, California

Comparisons between the yearly volume of steam withdrawn from The Geysers, California, geothermal reservoir and the number of earthquakes indicate that most of the seismicity is induced. To establish the inducing mechanism, an estimate of the stress field orientation was calculated from inversion of 210 fault plane solutions. Below 1 km depth The Geysers is undergoing uniaxial extension with the least principal stress σ_3 oriented near horizontal at approximately 105° azimuth. The consistency between the local and regional stress fields indicates that the regional tectonic stress is much larger than the stresses induced locally through geothermal activities. The stress data are equivocal as to whether earthquakes are induced due to conversion of aseismic to seismic slip or by increased shear stresses arising from reservoir contraction. The observed tendency for downward growth of seismicity may arise from a preferential fracture orientation that is near vertical in conjunction with a stress state where the gradient of σ_1 exceeds that of σ_3. Evidence of extension at The Geysers and in the surrounding Clear Lake region indicates a direct relationship to the presence of the Quaternary Clear Lake Volcanics.

INTRODUCTION

In an analysis of temporal and spatial distributions of seismicity at The Geysers, California, geothermal reservoir, *Eberhart-Phillips and Oppenheimer* [1984] demonstrated that activities related to steam withdrawal induced earthquakes. They speculated that the cause of the earthquakes could be explained by one of two mechanisms. The first involved stress perturbations related to volumetric contraction of the reservoir arising from the mass of fluid withdrawn from the reservoir [*Majer and McEvilly*, 1979] or from thermal contraction due to reservoir cooling [*Denlinger et al.*, 1981]. Alternatively, seismicity could be generated by conversion of aseismic deformation to stick-slip [*Allis*, 1982]. The style of faulting may confirm this hypothesis, if correct. With the former mechanism the induced stress field may be expected to have a radial component to it if the entire reservoir contracts uniformly. The latter mechanism would predict a stress field consistent with regional estimates. To discern which of these mechanisms is dominant, the orientation of the stress field at The Geysers is estimated through an analysis of a suite of 210 earthquake fault plane solutions distributed throughout the reservoir. The estimate of the stress field is then compared with geodetic measurements and geologic structure for its ability to resolve the inducing mechanism and regional tectonics.

EVIDENCE FOR INDUCED SEISMICITY

Since May 1975, earthquakes have been routinely located at The Geysers from *P* wave arrival times recorded with the U.S. Geological Survey's Central California Seismic Network (CALNET) (Figure 1). The locations are computed by the program HYPO71 [*Lee and Lahr*, 1975] using the one-dimensional velocity model of *Eberhart-Phillips and Oppenheimer* [1984] (Table 1). This model was determined through a joint hypocenter and velocity inversion, and the resulting location standard errors are considered to be within 0.3 km based on a comparison of locations of downhole explosions within the center of The Geysers. The uncertainty arises primarily from unmodeled lateral velocity variations within the region.

The evidence for induced seismicity at The Geysers is the temporal and spatial distribution of microearthquakes in the vicinity of producing steam wells. *Eberhart-Phillips and Oppenheimer* [1984] observed that during the period 1975–1981, earthquakes occurred in previously aseismic regions of The Geysers within months following the extraction of steam from newly developed regions of the reservoir. Between 1981 and 1984, steam production at The Geysers has expanded significantly by the addition of power plants SMUDGEO 1 (December 1983, NCPA 2 (September 1983), Sante Fe Geothermal (March 1984), and P.G. & E. units 17 (November 1982) and 18 (January 1983), all of which receive steam from previously undeveloped regions of the reservoir (Figure 2). Maps of seismicity in 3-year periods for magnitude (M) ≥ 1.2, the magnitude above which earthquake locations are complete since 1975, show that seismicity has also been induced adjacent to the above power plants (Figures 2*a*–2*c*). It is difficult to recognize induced seismicity at unit 18 above *M*1.2, although smaller earthquakes clearly indicate the phenomenon.

The earthquake activity extends from the surface to depths of 6.5 km, 3 km deeper than the maximum depths of steam wells in the reservoir [*Reed*, 1982] (Figure 3). Within the uncertainties of the locations and downhole position of the steam wells, most seismicity above 3.5 km depth is located within a few hundred meters laterally of the wells. The seismicity below 3.5 km depth occurs primarily in the region of The Geysers with the longest production history and is laterally distributed in a uniform fashion (Figure 2*d*).

Additional evidence for induced seismicity exists in the correlation between the yearly number of earthquakes of $M \geq 1.2$ and the amount of electric kilowatt-hours (kWh) generated for entire The Geysers geothermal reservoir for the period 1976–1984 (Table 2, Figure 4). This comparison also addresses the question of whether noninduced seismicity at The Geysers existed prior to development of the geothermal reservoir. The data represented in Figure 4 include production statistics and earthquake counts in the vicinity of the 11 power plants that were generating electricity prior to the beginning of seismic monitoring in May 1975, as well as data from those power plants where induced seismicity is recognized. Therefore the good correlation indicates that the seismicity occurring in the older producing regions of The Geysers is also induced and

Paper number 6B5957.

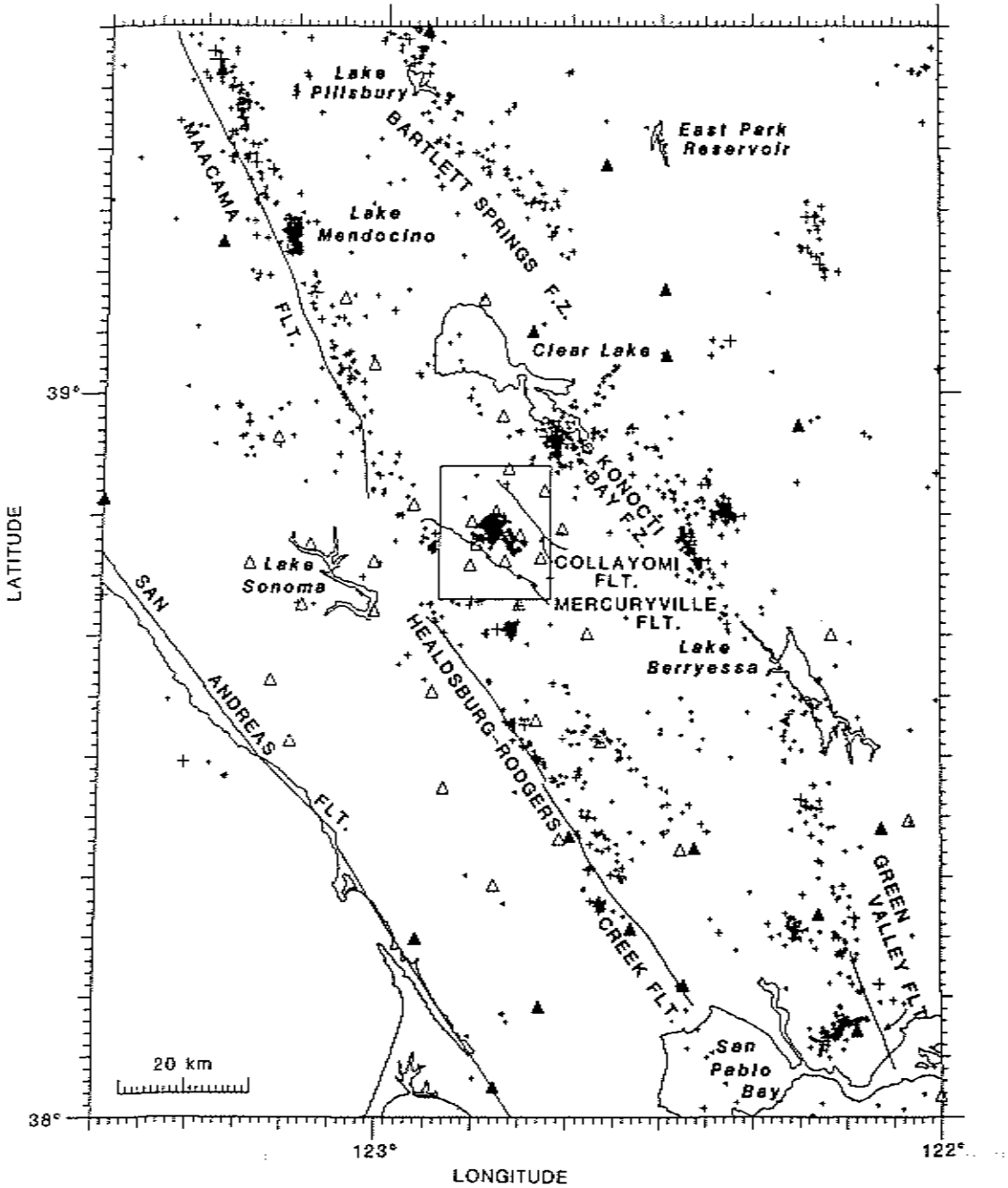

Fig. 1. Seismicity and fault map of The Geysers and surrounding region. Pluses outside of box represent earthquakes for time period January 1976 through December 1984 with $M \geq 1.5$ and quality A–C [*Lee and Lahr*, 1975]. Seismicity inside box depicts earthquake locations for which fault plane solutions have been determined in this study for time period January 1984 through October 1985. Open triangles depict locations of CALNET stations used in computation of fault plane solutions. Solid triangles depict locations of stations used only for location of regional seismicity. Many of the latter stations were not in operation during period of this study.

that there was likely very little earthquake activity in The Geysers region prior to withdrawal of steam. The correlation presented in Figure 4 substantiates the findings of *Marks et al.* [1978], who examined the number of earthquakes above *M*2.0 with *S-P* travel times consistent with earthquake locations within 60 km of the University of California's Calistoga seismic station. They found that the level of seismicity for the period 1975–1977 was about twice as high as for the preproduction period 1962–1963, and they also attributed the increase to the occurrence of induced seismicity at The Geysers.

TABLE 1. Velocity Model for The Geysers

Top of Layer, km	Layer Thickness, km	Velocity, km/s
0.00	1.50	4.43
1.50	1.50	5.12
3.00	1.25	5.47
4.25	1.75	5.58
6.00	2.00	5.62
8.00	12.00	5.86
20.00	...	7.95

Eberhart-Phillips and Oppenheimer [1984].

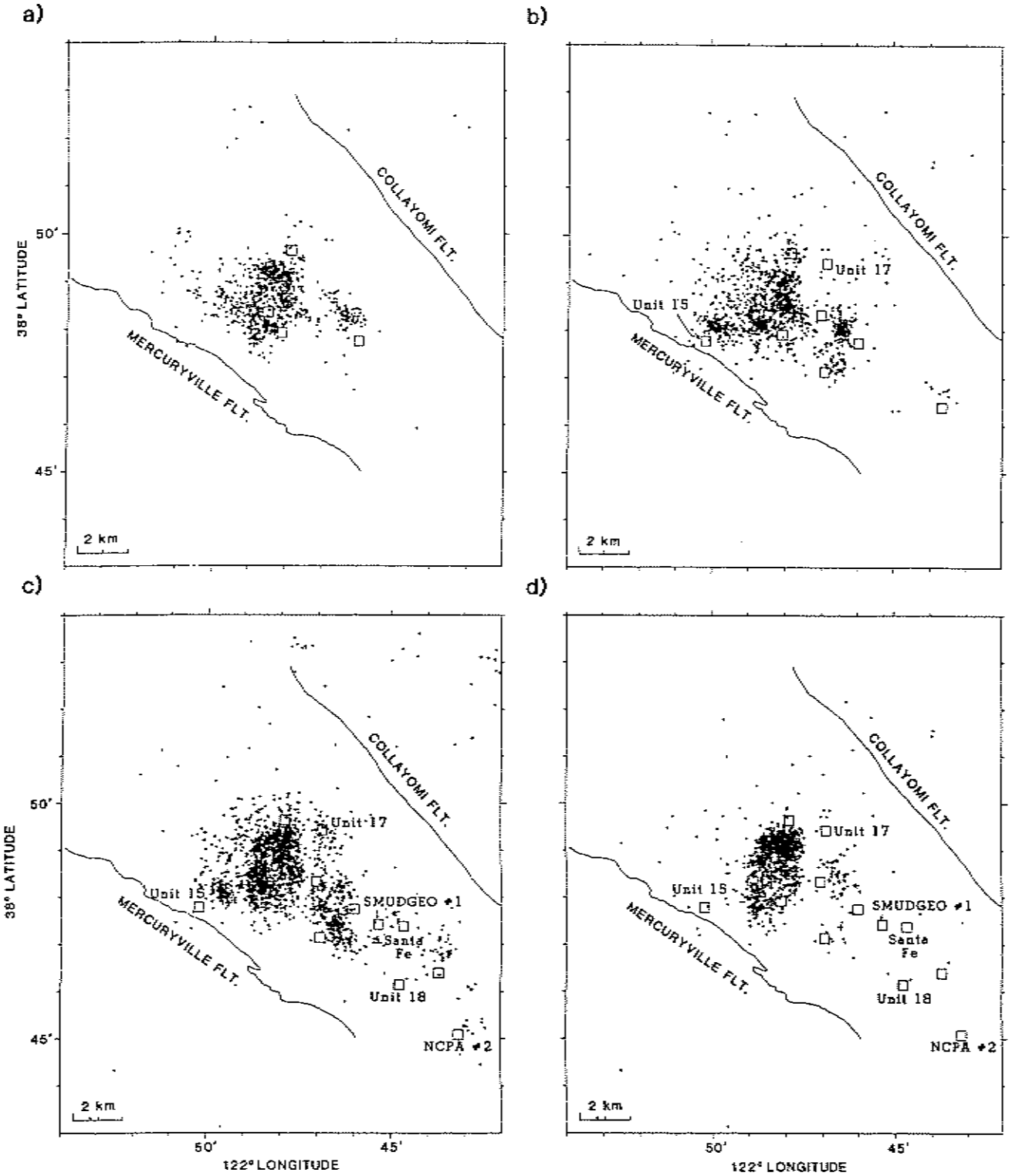

Fig. 2. Locations of earthquakes in The Geysers region with $M \geq 1.2$ and quality = A–C [*Lee and Lahr*, 1975] for the periods (*a*) 1976–1978, (*b*) 1979–1981, and (*c*) 1982–1984. Small open squares represent geothermal power plants in operation during time period. Note the increase in earthquake activity in previously aseismic regions as power plants began operation. (*d*) Seismicity deeper than 3.5 km for time period January 1976 through December 1984.

Eberhart-Phillips and Oppenheimer [1984] review a variety of inducing mechanisms to explain the seismicity at The Geysers and note that mechanisms associated with the reduction of effective normal stress [*Hubbert and Rubey*, 1959] are not likely. Since water within The Geysers reservoir is at saturation conditions, reservoir pressures follow the steam-static gradient. Production of steam from the reservoir has caused the steam pressure in the reservoir to decline of the order of 0.1 MPa/yr [*Lipman et al.*, 1978] which would tend to increase the effective normal stress on fault surfaces and inhibit slip. Similary, empirical correlations between the number of earthquakes and the volume of steam condensate injected into

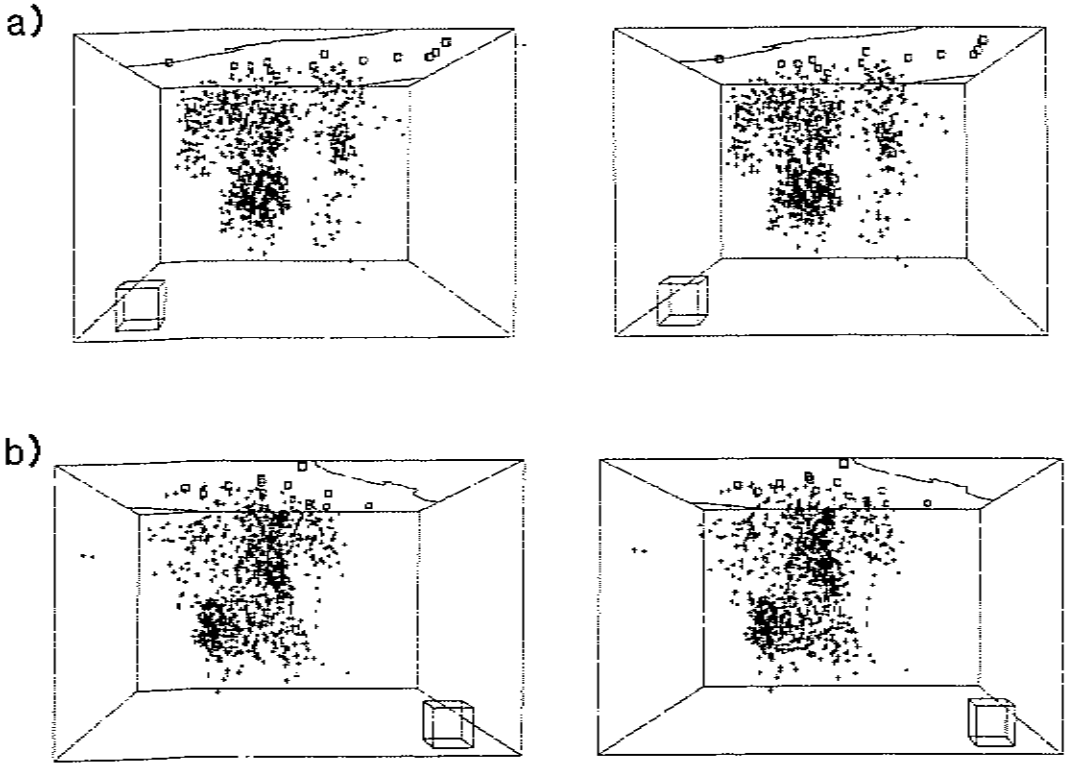

Fig. 3. Stereo projection of seismicity in The Geysers geothermal reservoir with $M \geq 1.5$, quality = A–C, and travel time residual rms ≤ 0.10 s [*Lee and Lahr*, 1975] for the period January 1976 through December 1984. Boxes at surface denote geothermal power plants in operation as of December 1984; lines at surface denote faults depicted in Figure 2. Large cube at depth is 1 km per side, and the depth of the plot is 7 km. Viewpoint is at a depth of 3 km from south in Figure 3*a* and east in Figure 3*b*.

the reservoir are statistically insignificant [*Eberhart-Phillips and Oppenheimer*, 1984], indicating that water injection is not the primary inducing mechanism. They conclude that two mechanisms remain plausible for inducing seismicity at The Geysers. The first mechanism involves increased shear stresses arising from volumetric contraction due to either thermal contraction or reservoir compaction from mass withdrawal. Alternatively, aseismic slip could be converted to seismic slip due to an increase in the coefficient of friction following the deposition of exsolved silica onto fracture surfaces [*Allis*, 1982].

FAULT PLANE SOLUTIONS

Fault plane solutions were computed via the grid search algorithm FPFIT which assumes a double-couple source mechanism and mimimizes the discrepancies between predicted and observed first-motion polarities [*Reasenberg and Oppenheimer*, 1985]. Fault plane solutions were computed only for earthquakes having at least 15 first-motion observations, as it was found that confidence limits became too large for mechanisms composed of fewer first motions. The data set was further restricted by rejecting solutions for which the first-motion data were primarily concentrated near nodal planes. The magnitude of the resulting data set ranges from 1.1 to 3.3 (appendix Table A1).[1]

These restrictions in no way ensure uniqueness in the computed fault plane solutions, and it is difficult to assess whether the solutions in appendix Figure A1 are "correct" in the sense that they correspond to the true orientation of the fault plane and slip direction. Figure 5 demonstrates the problem in the extreme. For these two earthquakes there is no way to differentiate between normal, strike-slip, and thrust behavior without first-motion amplitude information. Since amplitudes are not routinely available, earthquakes exhibiting multiple fault plane solutions were rejected from the analysis. Multiple solutions occurred most frequently for earthquakes with depths less than 1.5 km because of the paucity of upgoing rays having angles of incidence less than 45°. For these shallow earthquakes there was frequently an ambiguity between pure strike-slip and pure dip-slip mechanisms. Even though both normal and thrust solutions are presented here as "unique" for earth-

TABLE 2. Yearly Seismicity and Geothermal Production Statistics

Year	$\sum M_o$,* N m	Number of Events ($M \geq 1.2$)	Kilowatt-Hours Generated†	Net Mass H_2O Withdrawn,‡ kg
1976	5.0×10^{14}	464	3.7×10^{8}	2.4×10^{10}
1977	4.1×10^{14}	396	3.7×10^{8}	2.5×10^{10}
1978	3.7×10^{14}	325	3.1×10^{8}	2.1×10^{10}
1979	4.6×10^{14}	495	4.0×10^{8}	2.7×10^{10}
1980	6.4×10^{14}	760	5.3×10^{8}	3.6×10^{10}
1981	7.9×10^{14}	918	5.9×10^{8}	3.9×10^{10}
1982	1.6×10^{15}	625	5.1×10^{8}	3.6×10^{10}
1983	1.3×10^{15}	1060	6.7×10^{8}	4.6×10^{10}
1984	1.3×10^{15}	1147	9.5×10^{8}	5.5×10^{10}

*The seismic M_o is estimated from the U.S.G.S. coda duration magnitude M_D by $\log M_o = 1.2M_D + 17$ [*Bakun*, 1984].
†Pacific Gas and Electric (personal communication, 1985).
‡*California Department of Conservation* [1984].

[1]Appendix table and figure are available with entire article on microfiche. Order from American Geophysical Union, 2000 Florida Avenue, N.W., Washington, DC 20009. Document B86-005; $2.50. Payment must accompany order.

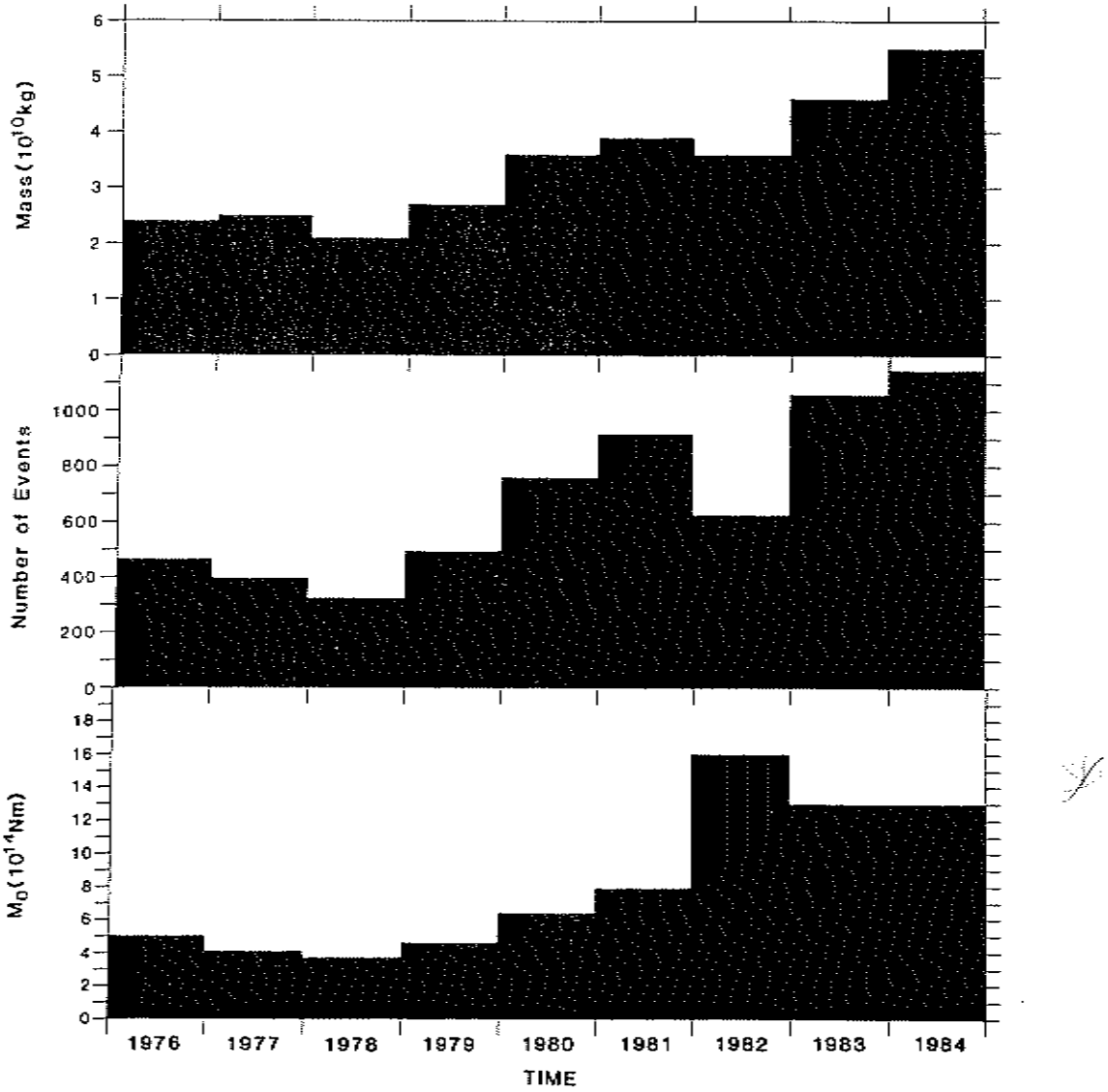

Fig. 4. Yearly net mass of water withdrawn compared with the yearly number of earthquakes $M \geq 1.2$ and quality = A–C [*Lee and Lahr*, 1975] and the associated moment sum (Table 2) for entire The Geysers geothermal reservoir. The presence of a few $M3+$ earthquakes greatly influences the moment sum calculation and explains the better correlation between yearly mass withdrawn and number of earthquakes.

quakes at depths less than 1.5 km, it should be recognized that considerable uncertainty exists as to the correct sense of slip for many of these solutions. Accordingly, the conclusions of this study are based on analysis of the ensemble of fault plane solutions rather than from the interpretation of a few, well-constrained solutions. The resulting 210 fault plane solutions which span the time period January 1984 through October 1985 are displayed in Figure 1 (see also Figure A1 on microfiche). Table A1 on microfiche contains the corresponding hypocentral and fault plane solution parameters sorted on depth.

While the earthquakes are relatively well located with a one-dimensional, flat-layered, uniform velocity model (Table 1), it is only an approximation to a known three-dimensional structure [*Eberhart-Phillips*, 1986*a*]. The inadequacy of the one-dimensional model is clearly demonstrated by the 5-km offset of earthquakes from the mapped trace of the Maacama fault in Figure 1. The computed ray paths may deviate from the actual path due to the depth position of layer boundaries, unmodeled velocity anomalies, and location errors. In particular, the azimuth and takeoff angles of upgoing rays for short ray paths are quite sensitive to mislocation errors. Many of the unresolved polarity discrepancies exhibited in the fault plane solutions may be attributed to the above causes in addition to the misidentification of the first-motion sense.

The solutions exhibit a variety of mechanisms ranging from normal to reverse slip over epicentral distances less than 2 km (Figure 6) and do not exhibit much spatial consistency in fault plane orientation. Given the variety of fault plane orientations, the lack of any detectable trends in hypocenter locations, and the generally small magnitudes ($M \leq 4.0$) at The Geysers [*Eberhart-Phillips and Oppenheimer*, 1984], the earthquakes appear to be occurring on small, randomly oriented, preexisting fractures.

Estimation of Principal Stress Axes Orientation

The P and T axes for all events are shown in Figure 7 and exhibit a large degree of scatter which may arise from several sources. First, the average uncertainty in computed fault plane orientation is easily 20° due to an inadequate station distri-

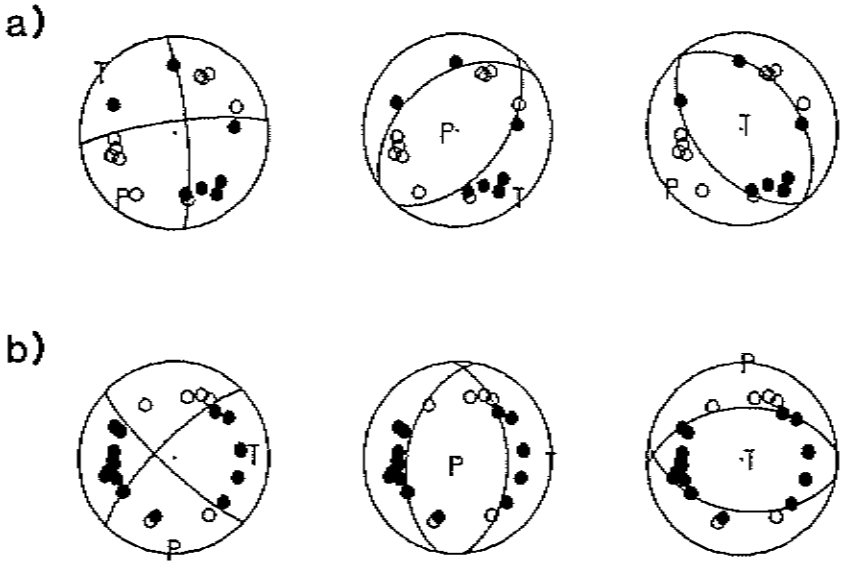

Fig. 5. Example of multiple fault plane solutions for shallow earthquakes at The Geysers. Lower hemisphere, equal-area projection fault plane solutions with corresponding P and T axes. Open circles are dilatations; solid circles are compressions. Note that the first-motion data are equally satisfied by either a strike-slip, normal, or reverse mechanism. (*a*) An $M2.5$ earthquake that occurred at a depth of 1.3 km on September 9, 1984, at 0208 UT, and (*b*) an $M1.7$ earthquake that occurred at a depth of 1.5 km on August 13, 1985, at 1829 UT.

bution, mislocation errors, unmodeled velocity anomalies, and errors in the reporting of first-motion polarities. Second, if failure is occurring on randomly oriented fractures in response to a consistent regional tectonic stress, the orientations of the P and T axes may depart from the orientation of the associated principal stress axes [*McKenzie*, 1969]. The variety of mechanisms shown in Figure A1 (on microfiche) is clearly not attributable to modeling uncertainties and confirms that the

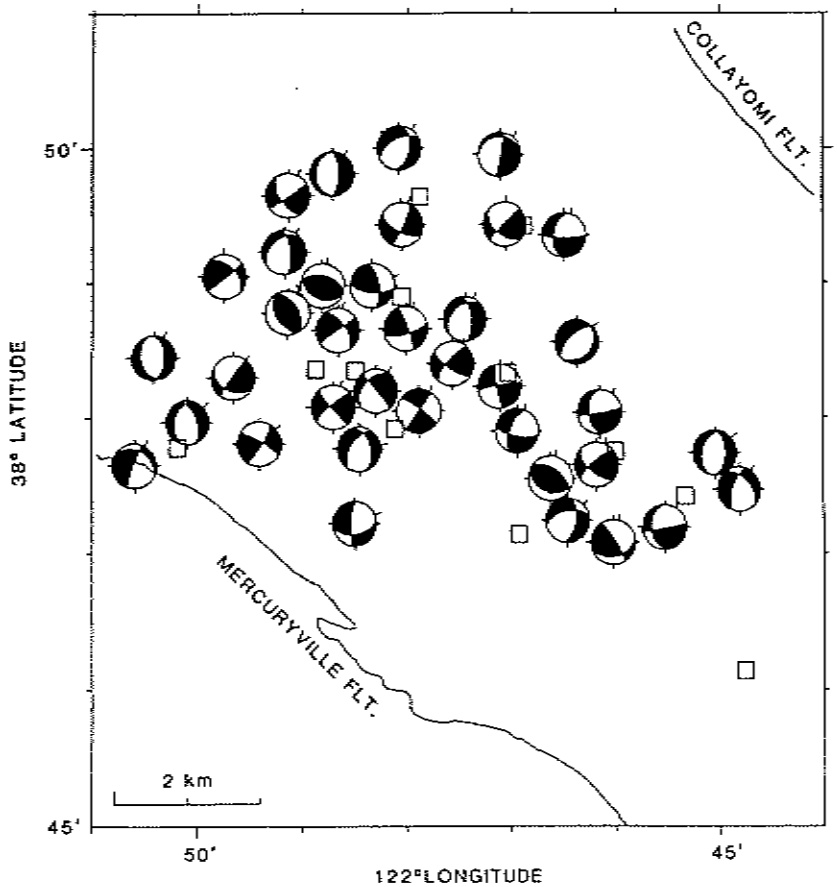

Fig. 6. Representative lower hemisphere, equal-area projection fault plane solutions. Shaded areas are compressional regions of focal sphere. Note random fault plane orientation and earthquakes exhibiting different styles of faulting over small epicentral distances. Area corresponds to stereo projections in Figures 3 and 8.

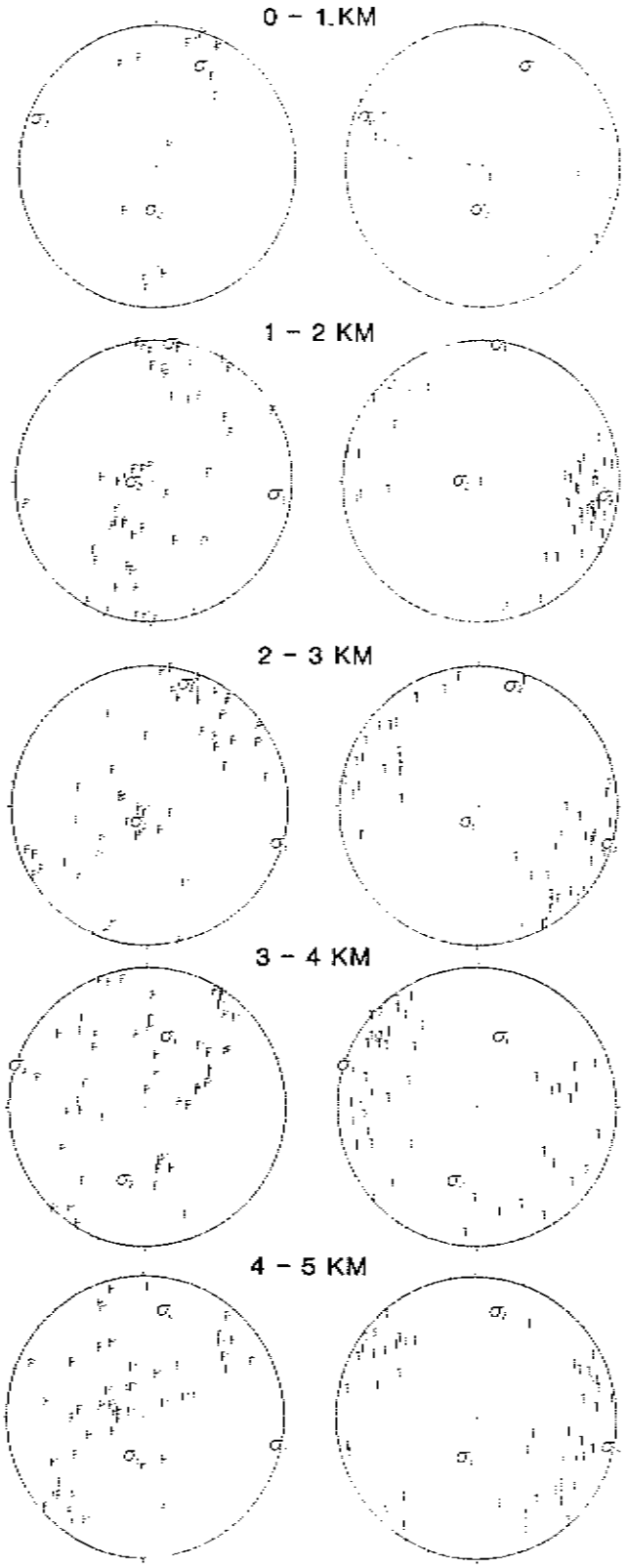

Fig. 7. P and T axes as a function of 1.0-km depth intervals corresponding to the fault plane solutions in Figure A1 on microfiche. Poles of principal stress axes for solution A calculated from inversion of fault plane solutions (Table 3) are also depicted. In the upper 1.0 km the P axes are horizontal oriented NNE-SSW, while the T axes range from vertical (reverse) to horizontal (strike-slip). At depths greater than 1.0 km the T axes are always horizontal oriented WNW-ESE, while the P axes range from horizontal to vertical (normal), suggesting that The Geysers is undergoing uniaxial extension at depth.

slip planes are not all oriented in the direction of maximum shear stress for a uniform stress field. Third, if the earthquakes are induced by stress perturbations associated with reservoir contraction and the magnitudes of the perturbations approach or exceed the magnitude of the regional stress, the resultant stress field may not be spatially uniform.

Within the scatter of the data, the orientations of the P and T axes in Figure 7 do not show much evidence of depth dependence. In the depth interval 0–1 km the P axes range from horizontal to vertical along a NNE-SSW azimuth, while the T axes also range from horizontal to vertical along an ESE-WNW azimuth. The fault plane solutions in this depth interval (1–14, Figure A1) exhibit normal, strike-slip, and reverse mechanisms. At depths from 1.0 to 3.0 km (15–63, Figure A1) the P axes range from horizontal to vertical. Except for one earthquake (27) at a depth of 1.34 km, the T axes are nearly horizontal along azimuths similar to the mechanisms at depths less than 1.0 km. Normal to oblique-normal slip is indicated by the mechanisms with significant nonhorizontal P and horizontal T axes. At depths greater than 3.0 km the P axes are predominantly nonhorizontal and do not appear to be azimuthally consistent. Despite the large degree of azimuthal scatter, the orientations of the T axes are generally more consistent than P axes and indicate that the intermediate principal stress σ_2 is approximately equal to the greatest principal stress σ_1.

If the induced stresses are assumed to be small in comparison to the regional stress and if the deformation is assumed to be due to the regional stress field, an estimate of the orientation and relative magnitudes of the principal stress axes can be found by inversion of the fault plane solutions [*Angelier*, 1984]. *Gephart* [1985] shows that for cases when σ_2 does not coincide with the B axis of the fault plane solution, traction on a fault plane for a given stress field is consistent with only one of the two possible slip directions of the fault plane solution. Thus it is desirable to specify the slip plane from the auxiliary in the inversion. Since there is little correspondence between earthquake locations and mapped faults at The Geysers [*Eberhart-Phillips and Oppenheimer*, 1984] and the epicenters do not clearly define any linear trends, the near-random orientation of fault planes makes the choice of slip plane generally impossible. Consequently, both of the possible fault planes were used as the data set for determination of the deviatoric component of the stress tensor.

Following *Angelier* [1984], the inversion procedure involves solving for the orientation of the principal stress axes and stress ratio ϕ defined as

$$\phi = \frac{\sigma_2 - \sigma_3}{\sigma_1 - \sigma_3} \qquad \sigma_1 \geq \sigma_2 \geq \sigma_3 \tag{1}$$

Initial estimates of the solution were obtained through an analytical least squares inversion that minimizes the function S_3 [*Angelier*, 1979],

$$S_3 = \sum_{k=1}^{K} \min\left[\tan^2(s_k, \Gamma_k), 1\right] \tag{2}$$

where K equals twice the number of fault plane solutions, s_k the observed slip vector, and Γ_k the shear stress. For those observations where the angle between the slip vector and shear stress exceeds 45°, $\tan(s_k, \Gamma_k)$ was set to unity to prevent observations which are inconsistent with the stress field from affecting the solution.

TABLE 3. Orientation and Relative Magnitudes of Principal Components of Stress Tensor

	Solution A*								Solution B†							
	σ_1		σ_2		σ_3				σ_1		σ_2		σ_3			
Depth, km	Azimuth	Plunge	Azimuth	Plunge	Azimuth	Plunge	ϕ	Coherence‡	Azimuth	Plunge	Azimuth	Plunge	Azimuth	Plunge	ϕ	Coherence‡
0.0–1.0	25	25	185	64	292	8	0.54	93	165	77	27	10	295	9	1.00	71
1.0–2.0	7	2	267	78	97	12	1.00	82	251	77	6	6	97	12	1.00	82
2.0–3.0	217	78	16	11	107	4	0.99	70	199	6	322	79	108	9	0.97	71
3.0–4.0	18	46	197	44	287	0	0.99	67	198	55	15	35	106	1	0.99	66
4.0–6.0	199	66	11	24	102	3	0.95	68	12	2	252	87	102	3	1.00	67

*Starting value of grid search is σ_1 and σ_3 of direct inversion [*Angelier*, 1979].
†Starting value of grid search is σ_2 and σ_3 of direct inversion.
‡Percentage of fault planes for which the angle between the predicted and observed slip directions $< 45°$.

Since the inverse problem is nonlinear, particularly in the presence of large data dispersion [*Angelier*, 1984], the results of the above "direct" inversion then served as initial values to an iterative inversion that again minimized S_3. This second inversion is a search over a four-dimensional grid described by the orientation of the three principal stress axes and ϕ. The iteration was terminated when the solution converged to within 3.5° of the previous iteration.

To investigate whether the orientation of the stress field varied with depth, the inversion was performed on the fault plane data divided into 1-km intervals corresponding to the P and T diagrams in Figure 7. The results show that $\phi \cong 1$ (i.e., $\sigma_1 \cong \sigma_2$) at depths greater than 1 km (Table 3), indicating that the stress tensor computed by the grid search procedure was dependent upon the initial values of the search. The consistency of the inversion results was then investigated by beginning the grid search with σ_2 and σ_3 of the direct inversion and comparing the resulting stress tensor with results from the previous inversion which used σ_1 as the initial value. The comparison shows that the iterative inversion converged to a stress orientation near the initial value with σ_3 unchanged, but with the orientation of σ_1 and σ_2 interchanged (Table 3).

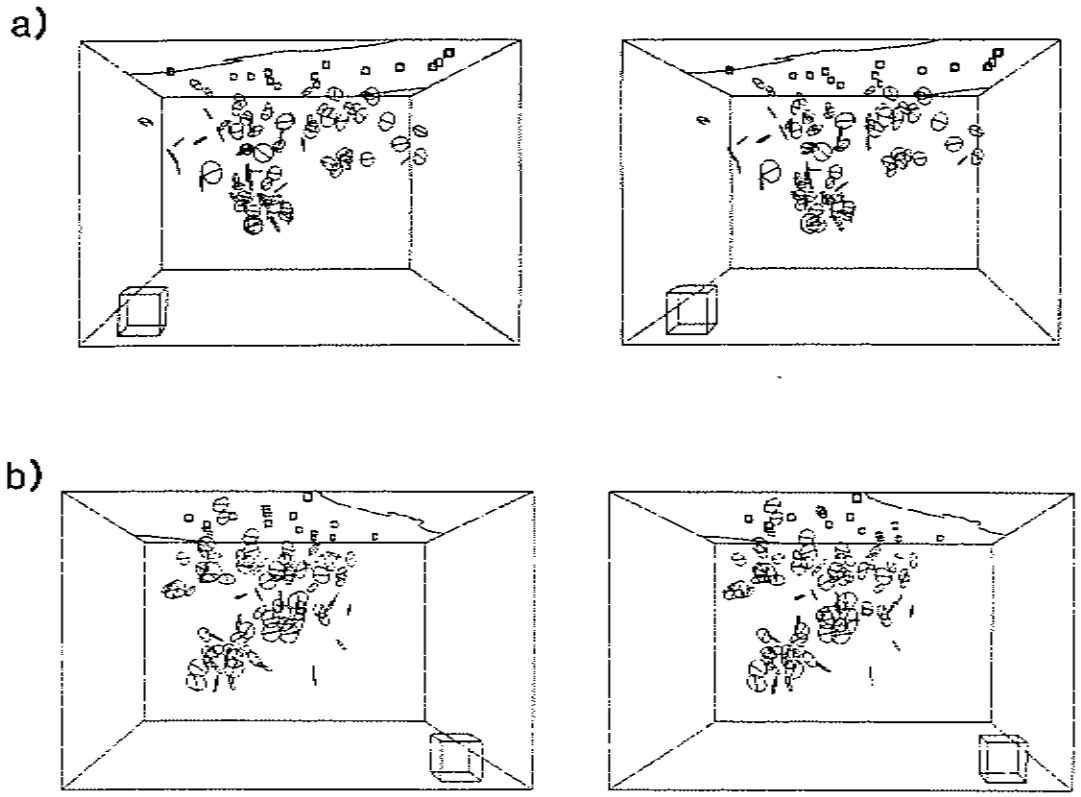

Fig. 8. Stereo projection of fault planes with slip vectors consistent with solution A stress field (Table 3). See Figure 3 for description of plot. For clarity, multiple fault planes are not plotted for earthquakes located within 0.40 km of another earthquake.

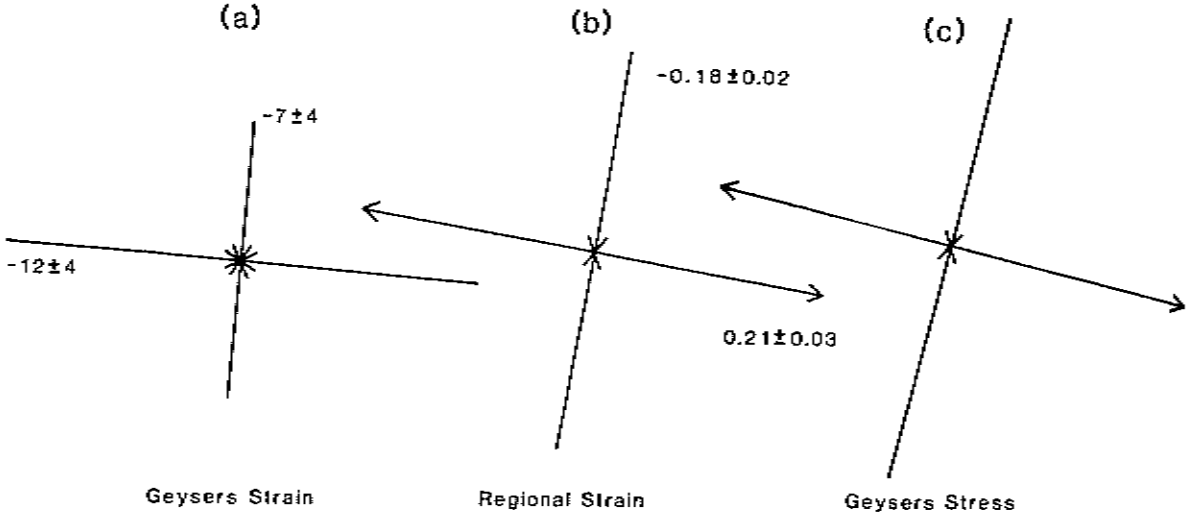

Fig. 9. Comparison between (*a*) local [*Denlinger et al.*, 1981] and (*b*) regional [*Prescott and Yu*, 1986] estimates of the horizontal principal strain rate (μstrain/yr), and (*c*) the horizontal projection of the orientation of the maximum and minimum stress axes averaged over the five depth intervals (Table 3). Since $\phi = 1$ for depths greater than 1 km, the axis σ_1 or σ_2 closest to horizontal is taken as the maximum principal stress axis. Note agreement between regional strain field and stress field at The Geysers. In contrast, the local strain field indicates contraction of the steam reservoir.

Although the data set consisted of both the slip and auxiliary fault planes, the minimization function S_3 eliminates one of the two planes from the inversion in most cases. Because the solution converged from different initial values to the same orientation of the principal stress axes values and same ϕ value (Table 3), the results of the stress orientation inversion appear to be insensitive to the specification of the slip plane.

The least and greatest principal stress axes locate near the corresponding mean of the P and T axes of Figure 7. This result supports the assumption of *Zoback and Zoback* [1980] that the average P and T orientations from a number of fault plane solutions tend to be reliable indicators of the principal stress orientations. Since the formal uncertainties associated with the fault plane solutions are unknown and both the slip and auxiliary planes serve as data for the inversion, there are no formal estimates of the inversion uncertainties for the orientations of the principal stress axes. However, the scatter of the P and T axes in Figure 7 represents a reasonable estimate of the uncertainty. The uncertainties associated with ϕ are unknown.

The inversion results help to explain why earthquakes located within 1 km of the surface exhibit reverse focal mechanisms. Since $\phi = 1$ below 1 km, the maximum horizontal compressive stress is approximately equal to the lithostatic load. Near the surface the lithostatic load will be small, σ_3 may become vertical, and σ_1 would be horizontal. Assuming that the normal faulting mechanisms observed above 1.0-km depth do not result from errors in the calculated hypocentral depth or errors in fault plane solution determination (Figure 5), the mechanisms may reflect the variable lithostatic load at common elevations due to the rugged topography at The Geysers (in excess of 0.5 km over lateral distances of 2.5 km).

The predicted shear stress resolved onto each set of slip and auxiliary fault planes can be calculated from the computed stress tensor and compared with the respective slip vectors of the fault plane solution. The plane with the smallest deviation angle between the resolved shear stress for solution A in Table 3 and the observed slip vector can be considered the plane that would slip under the computed stress field. These preferred planes are plotted in stereo perspective in Figure 8. The spatial consistency of the fault plane orientations provides some measure of the ability of the inversion to correctly indentify the slip plane. Fault planes for which the deviation angle exceeds 45° are excluded from Figure 8 as slip on these planes is inconsistent with the predicted stress field, and these angles are too large to be explained by errors in determining the mechanism. For clarity, the plot of the resulting set of 156 fault planes is further simplified by excluding earthquakes which are within 0.40 km of other earthquakes.

The 84 fault planes shown in Figure 8 exhibit very little throughgoing alignment. This lack of alignment may have several explanations. First, typical uncertainties of 0.3 km for the hypocentral locations and 20° in fault plane orientation could account for much of the disorder (see 1 km cube in Figure 8 for scale). Second, since only 156 out of 210 fault plane solutions have slip directions consistent with the computed stress field, it suggests that either the data set is inconsistent with the assumption of a uniform stress field and that the computed field is only an average estimate of a spatially varying field or that the uncertainties of the data are too large to obtain a consistent result. Third, the random style of faulting suggested in Figure 8 may indeed be representative of the way in which faulting occurs in The Geysers reservoir. The lack of fault plane alignment and the fact that $\phi = 1$ at depths greater than 1 km in this region makes it doubtful that the inversion has correctly identified the slip plane.

In an analysis of 17 earthquakes at The Geysers during the period August 1977 through December 1977, *Bufe et al.* [1981] noted that the dominant mode of faulting changed from strike-slip to normal following an $M3.7$ strike-slip event in The Geysers. They inferred that the earthquake caused a reduction in northeasterly compressive stress and permitted the lithostatic load to become the maximum compressive stress. In a stress field for which $\phi = 1$, both strike-slip and

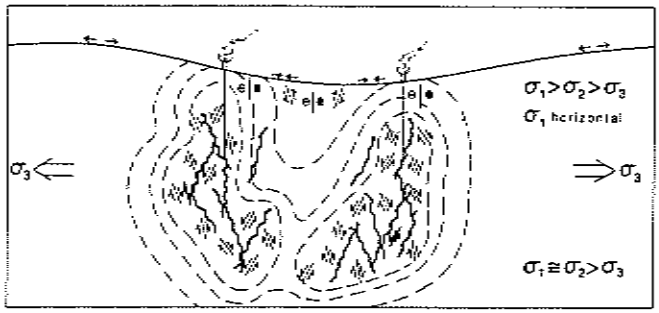

Fig. 10. Idealized model of induced strains at The Geysers. Dashes depict contours of equal strain. Contraction in the vicinity of fractures supplying steam to the wells may generate small stress perturbations on the order of a few tenths of a megapascal per year which are superimposed on the larger regional stress field. Short straight lines represent earthquake faults, and adjacent arrows represent sense of slip that arises from predominant regional shear stresses. Wavy solid lines represent fractures supplying steam to wells (light vertical lines). Bold arrows depict sense of regional tectonic extension. Induced seismicity at depths greater than the bottom of the steam wells may indicate communication between the wells and reservoir depths greater than 3.5 km by a system of deep, connected fractures.

normal faulting could occur, depending upon the orientation of the fault plane. Indeed, the comprehensive set of fault plane solutions presented in Figure A1 exhibits all manner of focal mechanisms which are unrelated to the order of occurrence. Because such variations appear to be the norm at The Geysers, this suggests that it is unnecessary to invoke temporal stress changes as an explanation for variations in focal mechanisms. Moreover, this illustrates that erroneous interpretations of the regional stress field may follow from analyses of small numbers of fault plane solutions in regions characterized by stress fields with ϕ values of 0 or 1.

Geodetic Data

To monitor crustal deformation associated with the earthquake process, The U.S. Geological Survey maintains a regional geodetic network spanning the Rogers Creek–Healdsburg fault zone and The Geysers region [*Prescott and Yu*, 1986]. The horizontal strain rates depicted in Figure 9 were calculated from an analysis of 32 lines for the period 1972–1983 and show a maximum principal strain rate of $+0.21 \pm 0.03$ μstrain/yr (extension) oriented N79° ± 2°W and a minimum principal strain rate of -0.18 ± 0.02 μstrain/yr (contraction) oriented N11° ± 2°E with an insignificant dilatation of $+0.03 \pm 0.03$ μstrain/yr [*Prescott and Yu*, 1986]. To compare the estimates of the principal strain rate axes from geodetic measurements with the stress axes obtained from the fault plane solutions, the horizontal projection of the orientation of the maximum and minimum stress axes averaged over the five depth intervals (Table 3) is plotted in Figure 9. Since $\phi = 1$ for depths greater than 1 km, the axis σ_1 or σ_2 closest to horizontal is taken as the maximum principal stress axis. There is good agreement between the horizontal components of the stress field and the regional strain field.

A local geodetic and leveling network was operated at The Geysers between 1973 and 1977 for the purposes of investigating production-related subsidence and contraction [*Lofgren*, 1981]. *Denlinger and Bufe* [1982] analyzed five electronic distance measurement lines spanning The Geysers. They found that the local horizontal strain rate is 1–2 orders of magnitude larger than the regional strain rate (Figure 9). It is difficult to identify the orientation of the principal strain rate axes due to the large uncertainties in the calculations, but unlike the regional strain field, the local east-west strain rate is clearly compressional. *Lofgren* [1981] also showed in his analysis of the leveling data that the region between the Mercuryville and Collayomi faults is subsiding as much as 2 cm/yr. Within The Geysers steam reservoir the subsidence rate increases to 3.4 cm/yr. Since the area of maximum subsidence correlates with the location of the maximum steam pressure decline in the reservoir [*Lipman et al.*, 1978], Lofgren speculated that the localized subsidence is induced. Similarly, *Denlinger et al.* [1981] were able to model the ratio of elevation changes to horizontal contraction in terms of reservoir contraction arising from the withdrawal of steam.

These geodetic studies demonstrate that the local strain field at The Geysers differs from the regional field. The local geodetic and leveling data show radial horizontal contraction coupled with rapid subsidence which indicates volumetric contraction of the reservior. In contrast, the region between the Maacama fault and Clear Lake shows NNE-SSW contraction and ESE-WNW extension with subsidence at a slower rate. The regional strain field is compatible with the results of the analysis of fault plane solutions, but the local strain field at The Geyser is not. This indicates that the faulting is driven by regional shear stresses which existed prior to the withdrawal of steam and which are larger than any locally induced shear stresses that may trigger earthquakes.

While the locally induced stress field may not be observed in the overall style of faulting, the state of stress at The Geysers is a combination of both induced and existing regional stresses. The stresses causing reservoir contraction would be radially oriented toward the center of subsidence and would result in compressive stresses near the center and extension on the edges of the reservoir (Figure 10). Similar results were observed to occur at the Wilmington oil field [*Yerkes and Castle*, 1976]. The spatial and temporal quality of the subsidence and geodetic data are not sufficient to accurately predict the magnitude of the induced stress field. Nonetheless, it is likely that in some areas of The Geysers the induced stresses would enhance slip on favorably oriented faults, while in other areas the induced stresses would inhibit slip.

Implications for Earthquake Inducing Mechanisms

The fault plane solution data demonstrate that the regional stress field predominates over the locally induced stress field at The Geysers. This observation supports the hypothesis that the earthquakes are induced by conversion of aseismic to stick-slip behavior due to an increase in the coefficient of friction from the deposition of exsolved silica on fault surfaces [*Allis*, 1982]. However, these observations do not preclude the alternate hypothesis that earthquakes are triggered by small stresses arising from reservoir contraction. For this mechanism the fault plane solution data require that triggering shear stresses be smaller than the regional shear stresses. The magnitude of these triggering stresses can be estimated from the local strain data. Assuming a Poisson's ratio of 0.29 [*Gupta et al.*, 1982], a mean density of 2.67×10^3 kg/m^3 [*Denlinger and Kovach*, 1981], and a mean compressional velocity of 5.5 km/s [*Eberhart-Phillips and Oppenheimer*, 1984], the modulus of rigidity is 2.4×10^4 MPa. Thus the shear stress perturbations corresponding to the local horizontal shear strain rates of 10^{-5}/yr are of the order of 0.2–0.3 MPa/yr. Since earthquake activity is generally induced within 6 months following the

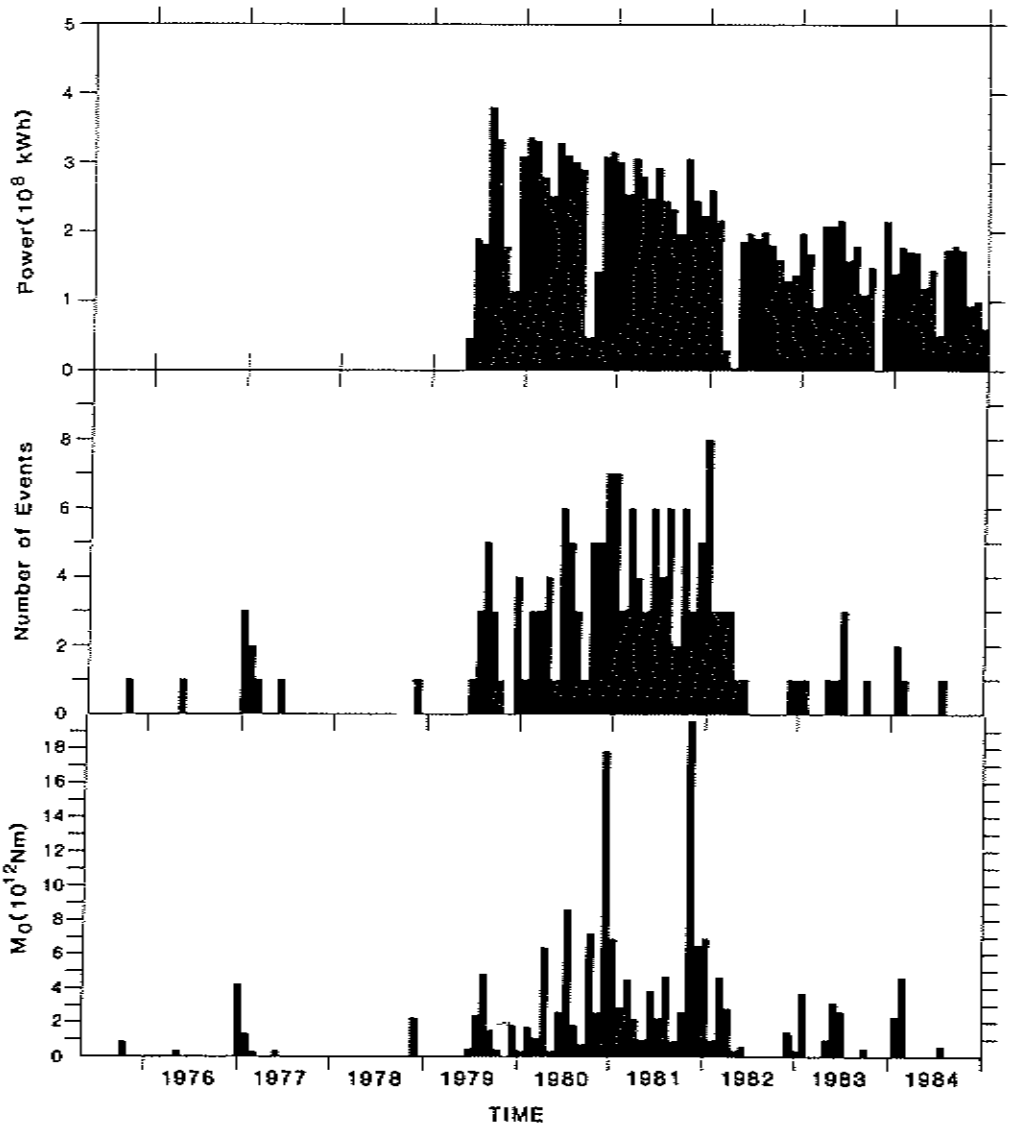

Fig. 11. Monthly number of kWh electricity generated at P.G. & E. unit 15 (Pacific Gas and Electric, personal communication, 1985) compared with the number of earthquakes $M \geq 1.2$ and quality = A–C [*Lee and Lahr*, 1975] per month and the associated moment sum. Note increase of seismicity following commencement of power generation and subsequent abatement of seismicity following the decrease in the number of kWh generated.

beginning of steam withdrawal, the locally induced stresses are only of the order of a few megapascals.

It follows from either of the two suggested inducing mechanisms that the shear stress at The Geysers must have been close to the failure condition prior to development of the steam reservoir. This is obvious if The Geysers was initially deforming aseismically. On the other hand if the earthquakes are induced by small stress perturbations associated with reservoir contraction, the amount of stress that could accumulate in the typical 6-month interval between commencement of production and recognized induced seismicity is shown above to be quite small. Laboratory measurements of rock samples from The Geysers by *Lockner et al.* [1982] show that the intact shear strength of the rock is so weak that it almost equals the frictional strength of the rocks. Consequently, the shear stresses at The Geysers are limited by the frictional strength of the rock; this explains why the predevelopment shear stress at The Geysers is close to failure.

Eberhart-Phillips and Oppenheimer [1984] speculate that time may be the most useful discriminant of all. After geothermal production ceases, Allis' mechanism would predict the cessation of earthquake activity only after the coefficient of friction declined to the value prior to development of the steam reservoir. Alternatively, if the earthquakes are the result of stress perturbations due to reservoir contraction, they speculate that the seismicity would abate within approximately 6 months following the cessation of steam withdrawal (i.e., equivalent to the time interval from when steam is first withdrawn to when induced seismicity is recognized). Figure 11 shows that the seismicity within 1 km of P.G. & E. unit 15 (Figure 2) has declined in response to the declining volume of steam withdrawn, indicated by the declining number of kWh generated at unit 15 (steam production data are proprietary). While this is currently the only example of this phenomenon, this finding suggests that reservoir contraction is the dominant mechanism for inducing earthquakes.

DEEP EARTHQUAKES

Approximately 30% of the earthquakes of $M \geq 1.2$ locate deeper than 3.5 km (Figure 2*d*), the maximum depth of well penetration at The Geysers [*Reed*, 1982]. Given the horizontal, east-west orientation of σ_3 (Figure 7, Table 3), the preferential orientation of open fractures from which steam is withdrawn should be near vertical and north-south. Supporting evidence comes from *Lipman et al.* [1978], who report that fracture orientations in drill cores from The Geysers are nearly vertical. Since most of the earthquakes are induced due to steam withdrawal, the "deep" seismicity indicates steam withdrawal from reservoir depths as great as 6 km via a system of permeable, vertically oriented fractures.

Figure 2 also shows that seismicity is not induced at distances greater than several hundred meters laterally from the wells. The distribution of earthquakes suggests that the induced seismicity is propagating downward. Downward growth of induced seismicity was also observed during fluid injection at the Cornwall, United Kingdom, hot dry rock site by *Batchelor et al.* [1983]. Although the inducing mechanism at The Geysers is not the result of fluid injection, *Pine and Batchelor's* [1984] explanation for the downward growth at Cornwall may also be applicable to The Geysers. They postulate that when slip occurs on a vertical plane, a component of the fracture growth will be in the vertical direction. If the incremental shear stress required for failure is greater in the upward direction, the fracture will tend to propagate downward. Since the shear stress is defined as

$$\tau = \frac{\sigma_{1_e} - \sigma_{3_e}}{2} \sin 2\theta \qquad (3)$$

where θ defines the angle between σ_1 and the fracture plane and the subscript e indicates effective stress, the fracture will tend to propagate downward if the local gradient of σ_{1_e} exceeds that of σ_{3_e}.

Given that $\phi = 1$ and σ_3 is horizontal, the gradient of σ_1 is equivalent to the lithostat. Estimates of the gradient of σ_3 can be made by assuming a coefficient of friction of 0.68 and that shear stresses in the reservoir are limited by the shear strength of the rock [*Lockner et al.*, 1982]. However, estimates of effective stress are much more uncertain, owing to the complex system of steam-dominated fractures and water-saturated pores [*Pruess and Narasimhan*, 1982]. The fault plane solution data demonstrate that the fracture orientation, expressed as θ, is also impossible to predict (Figure 6). Thus the data are not sufficient to confirm whether changes in the effective principal stress gradients cause the downward propagation of seismicity at The Geysers. If the seismicity does propagate downward, then it indicates that the induced seismicity is actively extending the vertical fracture system and enlarging the source region of steam withdrawal.

IMPLICATIONS FOR REGIONAL TECTONICS

The orientation of the extensional stress state at The Geysers is consistent with several prominent geologic features in the region. The Quaternary Clear Lake Volcanics overlie and obscure many of the vents and dikes, whose orientation could indicate the direction normal to σ_3 [*Nakamura*, 1977]. However, *Hearn et al.* [1981] note the existence of two zones of approximately N-S to N10°E trending volcanic eruptions. The first zone is located 5 km west of the Konocti Bay fault zone (Figure 1) and consists of basaltic andesite vents 0.6–0.35 m.y. age. The second zone is located just east of Clear Lake and consists of mafic cinder cones less than 0.1 m.y. In the vicinity of Mount St. Helena, 15 km southwest of The Geysers, 28 dikes of the Sonoma Volcanics (late Miocene to Pliocene) exhibit an average orientation of N14°E [*Fox*, 1983]. The orientation of σ_3, averaged over the five depth intervals of the inversion (Table 3), is N105°E and agrees with the dike and vent alignments.

Earthquake locations on both the Rogers Creek–Healdsburg-Maacama and the Green Valley–Bartlett Springs fault zones (Figure 1) define linear trends indicative of strike-slip faulting, as do most reliable fault plane solutions [*Bufe et al.*, 1981; *Dehlinger and Bolt*, 1984; *Warren et al.*, 1985]. However, the region bounded by the Maacama and Bartlett Springs fault zones is characterized by many localized regions of extension that appear to arise from the complex interaction of a system of echelon northwest oriented, right-lateral strike-slip faults [*Aydin and Nur*, 1982]. The most noteworthy are the 0.6 m.y. Clear Lake basin [*Hearn et al.*, 1981] and the 2.9–1.5 m.y. Cache Formation basin [*Rymer*, 1981] which are subsidence features arising from extension. Geologic mapping by *Hearn et al.* [1981] also indicates normal faulting to the south of Clear Lake between the Collayomi and Konocti Bay fault zones. Fault plane solutions indicate extension at The Geysers (this study) and the Konocti Bay regions [*Eberhart-Phillips*, 1986*b*].

The extensional environment at The Geysers is not easily recognized from the sense of offset of Tertiary and Quaternary fault movement above the reservoir; most mapped faults exhibit predominantly northwest trending, right-lateral strike-slip behavior [*McLaughlin*, 1981], which is consistent with the lack of lithostatic load near the surface. Furthermore, The Geysers geothermal reservoir underlies the axis of the Mayacamas Mountains which exhibits rugged topography and large elevation changes as noted earlier. This demonstrates that the extension does not have any geomorphic expression. Since it is only by virtue of the induced seismicity at The Geysers that extension is detectable, this raises the possibility that the entire region between the Rodgers Creek–Healdsburg and Bartlett Springs fault systems is undergoing extension.

A difficulty with the hypothesis of region-wide extension between the Rodgers Creek–Healdsburg and Bartlett Springs fault systems is the absence of either a major right-stepping offset or fault bend connecting the two sets of presumed dextral strike-slip master faults (Figure 1). *Eberhart-Phillips* [1986*b*] notes the NE-SW trend of seismicity between The Geysers and the southeast arm of Clear Lake which would suggest such an offset, but was unable to correlate this seismicity with any known geologic feature. However, if all of the seismicity which is induced at The Geysers is discounted, this lineation becomes much less pronounced. In addition, both master fault systems appear not only to bound the inferred region of extension but to extend well beyond the region as indicated by the seismically active Maacama and Green Valley faults. It should be recognized, however, that the occurrence of microseismicity by itself is not necessarily an indicator of large displacements through time, a fact that is easily demonstrated by the almost total absence of microseismicity on the San Andreas fault in Figure 1. It is possible that over time larger displacements occur on the Rodgers Creek–Healdsburg and Bartlett Springs fault systems than on the Maacama and Green Valley faults.

Finally, *Johnson and O'Neil* [1984] propose that volcanic activity in the Coast Ranges arises from mantle upwelling following the northward migration of the Mendocino triple junction [*Dickinson and Snyder*, 1979] and that volcanism occurs in regions in which the state of stress is moderately

compressive instead of extensional. The results presented in this study clearly show this not to be the case. The presence of Quaternary volcanism [*Donnelly-Nolan et al.*, 1981] and geophysically detected magma bodies [*Isherwood*, 1976; *Oppenheimer and Herkenhoff*, 1981] in The Geysers–Clear Lake region indicates that volcanism in the northern California Coast Ranges occurs in regions of tectonic extension.

CONCLUSIONS

The induced earthquake activity at The Geysers occurs on fault planes whose orientation is random and varies rapidly over short epicentral distances. Most fault plane solutions exhibit strike-slip to normal focal mechanisms, but earthquakes which locate above 1-km depth also exhibit reverse mechanisms. The estimate of the orientation and relative magnitudes of the principal components of the stress field from the fault plane data shows that The Geysers is undergoing uniaxial extension below 1 km with σ_3 oriented horizontally at approximately 105° azimuth. At depths less than 1 km the lithostatic load may be less than the maximum horizontal compressive stress, giving rise to a stress field in which σ_1 is oriented near horizontal at an azimuth of N26°E and σ_3 may range from vertical to horizontal at azimuths similar to estimates below 1 km.

The agreement between the orientation of the regional principal strain rate axes and the stress field orientation from the fault plane solutions demonstrates that any stress perturbations due to reservoir contraction are small in comparison to the magnitude of the regional tectonic stress field. If contraction is the primary inducing mechanism, the resulting stress perturbations induce earthquakes by triggering slip in the direction of the regional shear stress. The fault plane solution data are equally consistent with the hypothesis that the induced seismicity results from the conversion of aseismic to stick-slip movement due to the increase of the coefficient of friction from the deposition of exsolved silica on the fracture surfaces.

Earthquakes are induced at depths up to 3 km deeper than the bottom of the wells but generally at distances of only a few hundred meters laterally. Since most of the earthquakes are induced by the withdrawal of steam, the deep seismicity represents steam communication between the wells and deep regions of the geothermal reservoir through an extensive fracture network. The preferential downward growth of seismicity may result from the effective stress gradient of σ_1 exceeding that of σ_3, but the data on pore pressures and fracture orientation are insufficient at present to confirm this hypothesis.

The estimates of the stress field orientation from the seismic data are consistent with both the orientation and sense of slip of Quarternary faults and alignment of volcanic vents and cinder cones in The Geysers–Clear Lake region. The presence of large depositional basins to the north-northeast of The Geysers, together with the normal focal mechanisms observed at The Geysers and Konocti Bay fault zones, suggest that localized zones of extension occur throughout the region between the Maacama and Bartlett Springs fault zones. This study also demonstrates that it is difficult to identify extension at The Geysers on the basis of either topographic expression or the sense of slip on mapped faults, which are predominantly strike-slip due to the small lithostatic load near the surface. Finally, the presence of Quaternary volcanism throughout this region indicates that volcanism in the northern California Coast Ranges is associated with tectonic extension.

Acknowledgments. I am grateful to Rick Allis, Julie Donnelly-Nolan, Donna Eberhart-Phillips, Mike Fehler, Fred Klein, and Mary Lou Zoback for reviewing the manuscript and to Paul Reasenberg, Paul Segall, and Andrew Michael for many helpful discussions and suggestions. Mary Lou Zoback kindly provided the inversion routines for the estimation of the stress field orientation, and P.G. & E. provided production statistics for the geothermal power plants.

REFERENCES

Allis, R. G., Mechanism of induced seismicity at The Geysers geothermal reservoir, California, *Geophys. Res. Lett.*, *9*, 629–632, 1982.

Angelier, J., Determination of the mean principal directions of stresses for a given fault population, *Tectonophysics*, *56*, T17–T26, 1979.

Angelier, J., Tectonic analysis of fault slip data sets, *J. Geophys. Res.*, *89*, 5835–5848, 1984.

Aydin, A., and A. Nur, Evolution of pull-apart basins and their scale independence, *Tectonics*, *1*, 91–105, 1982.

Bakun, W. H., Seismic moments, local magnitudes, and coda-duration magnitudes for earthquakes in central California, *Bull. Seismol. Soc. Am.*, *74*, 439–458, 1984.

Batchelor, A. S., R. Baria, and K. Hearn, Monitoring the effects of hydraulic stimulation by microseismic event location: A case study, paper presented at the 58th Annual Technical Conference and Exhibition, Soc. of Pet. Eng., San Francisco, Calif., 1983.

Bufe, C. G., S. M. Marks, F. W. Lester, R. S. Ludwin, and M. C. Stickney, Seismicity of The Geysers–Clear Lake region, *U.S. Geol. Surv. Prof. Pap.*, *1141*, 129–137, 1981.

California Department of Conservation, Division of Oil and Gas, 70th Annual Report of the State Oil and Gas Supervisor, *Publ. PR06*, Sacramento, 1984.

Dehlinger, P., and B. A. Bolt, Seismic parameters along the Bartlett Springs fault zone in the Coast Ranges of northern California, *Bull. Seismol. Soc. Am.*, *74*, 1785–1798, 1984.

Denlinger, R. P., and C. G. Bufe, Reservoir conditions related to induced seismicity at The Geysers steam reservoir, northern California, *Bull. Seismol. Soc. Am.*, *72*, 1317–1327, 1982.

Denlinger, R. P., and R. L. Kovach, Three-dimensional gravity modeling of The Geysers hydrothermal system and vicinity, northern California, *Geol. Soc. Am. Bull.*, *92*, 404–410, 1981.

Denlinger, R. P., W. F. Isherwood, and R. L. Kovach, Geodetic analysis of reservoir depletion at The Geysers steam field in northern California, *J. Geophys. Res.*, *86*, 6091–6096, 1981.

Dickinson, W. R., and W. S. Snyder, Geometry of triple junctions related to San Andreas transform, *J. Geol.*, *87*, 609–627, 1979.

Donnelly-Nolan, J. M., B. C. Hearn, Jr., G. H. Curtis, and R. E. Drake, Geochronology and evolution of the Clear Lake Volcanics, *U.S. Geol. Surv. Prof. Pap.*, *1141*, 47–60, 1981.

Eberhart-Phillips, D., Three-dimensional velocity structure in northern California Coast Ranges from inversion of local earthquake arrival times, *Bull. Seismol. Soc. Am.*, in press, 1986*a*.

Eberhart-Phillips, D., Seismicity in the Clear Lake area, California, 1975–1982, Cores from Clear Lake: Late Quaternary Record of Climate, Tectonics, and Lake Sedimentation in the Northern California Coast Ranges, edited by J. D. Sims, *Spec. Pap. Geol. Soc. Am.*, in press, 1986*b*.

Eberhart-Phillips, D., and D. H. Oppenheimer, Induced seismicity in The Geysers geothermal area, California, *J. Geophys. Res.*, *89*, 1191–1207, 1984.

Fox, K. F., Tectonic setting of Late Miocene, Pliocene, and Pleistocene rocks in part of the Coast Ranges north of San Francisco, California, *U.S. Geol. Surv. Prof. Pap.*, *1239*, 33 pp., 1983.

Gephart, J. W., Principal stress directions and the ambiguity in fault plane identification from focal mechanisms, *Bull. Seismol. Soc. Am.*, *75*, 621–625, 1985.

Gupta, H. K., R. W. Ward, and T. L. Lin, Seismic wave velocity investigation at The Geysers geothermal field, California, *Geophysics*, *47*, 819–824, 1982.

Hearn, B. C., Jr., J. M. Donnelly-Nolan, and F. E. Goff, The Clear Lake Volcanics: Tectonic setting and magma sources, *U.S. Geol. Surv. Prof. Pap.*, *1141*, 25–45, 1981.

Hubbert, M. K., and W. W. Rubey, Role of fluid pressure in mechanics of overthrust faulting, *Geol. Soc. Am. Bull.*, *70*, 115–166, 1959.

Isherwood, W. F., Gravity and magnetic studies of The Geysers–Clear Lake geothermal region, California, in *Proceedings of the Second United Nations Symposium on the Development and Use of Geothermal Resources*, vol. 2, pp. 1065–1073, Lawrence Berkeley Laboratory, University of California, Berkeley, Calif., 1976.

Johnson, C. M., and J. R. O'Neil, Triple junction magmatism: A geochemical study of Neogene volcanic rocks in western California, *Earth Planet. Sci. Lett.*, *71*, 241–262, 1984.

Lee, W. H. K., and J. C. Lahr, HYPO71 (Revised): A computer

program for determining hypocenter, magnitude and first motion pattern of local earthquakes, *U.S. Geol. Surv. Open File Rep., 75-311*, 114 pp., 1975.

Lipman, S. C., C. J. Strobel, and M. S. Gulati, Reservoir performance of The Geysers field, *Geothermics, 7*, 209–219, 1978.

Lockner, D. A., R. Summers, D. Moore, and J. D. Byerlee, Laboratory measurements of reservoir rock from The Geysers geothermal field, California, *Int. J. Rock Mech. Min. Sci. Geomech. Abstr., 19*, 65–80, 1982.

Lofgren, B. E., Monitoring crustal deformation in The Geysers–Clear Lake region, *U.S. Geol. Surv. Prof. Pap., 1141*, 139–148, 1981.

Majer, E. L., and T. V. McEvilly, Seismological investigations at The Geysers geothermal field, *Geophysics, 44*, 246–269, 1979.

Marks, S. M., R. S. Ludwin, K. B. Louie, and C. G. Bufe, Seismic monitoring at The Geysers geothermal field, California, *U.S. Geol. Surv. Open File Rep., 78-798*, 43 pp., 1978.

McKenzie, D. P., The relation between fault plane solutions for earthquakes and the directions of the principal stresses, *Bull. Seismol. Soc. Am., 59*, 591–601, 1969.

McLaughlin, R. J., Tectonic setting of pre-Tertiary rocks and its relation to geothermal resources in The Geysers–Clear Lake area, *U.S. Geol. Surv. Prof. Pap., 1141*, 3–23, 1981.

Nakamura, K., Volcanoes as possible indicators of tectonic stress orientation—Principle and proposal, *J. Volcanol. Geotherm. Res., 2*, 1–16, 1977.

Oppenheimer, D. H., and K. E. Herkenhoff, Velocity-density properties of the lithosphere from three-dimensional modeling at The Geysers–Clear Lake region, *J. Geophys. Res., 86*, 6057–6065, 1981.

Pine, R. J., and A. S. Batchelor, Downward migration of shearing in jointed rock during hydraulic injections, *Int. J. Rock Mech. Min. Sci. Geomech. Abstr., 21*, 249–263, 1984.

Prescott, W. H., and S. Yu, Geodetic measurement of horizontal deformation in the northern San Francisco Bay region, California, *J. Geophys. Res., 91*, 7475–7484, 1986.

Pruess, K., and T. N. Narasimhan, On fluid reserves and the production of superheated steam from fractured, vapor-dominated geothermal reservoirs, *J. Geophys. Res., 87*, 9329–9339, 1982.

Reasenberg, P., and D. Oppenheimer, FPFIT, FPPLOT, and FPPAGE: Fortran computer programs for calculating and displaying earthquake fault-plane solutions, *U.S. Geol. Surv. Open File Rep., 85-739*, 109 pp., 1985.

Reed, M. J., Data for geothermal wells in The Geysers–Clear Lake area of California as of November 1980, *Spec. Rep. 11*, 37 pp., Geotherm. Resour. Counc., Davis, Calif., 1982.

Rymer, M. J., Stratigraphic revision of the Cache Formation (Pliocene and Pleistocene), Lake County, California, *U.S. Geol. Surv. Bull., 1502-C*, 35 pp., 1981.

Warren, D. H., C. Scofield, and C. G. Bufe, Aftershocks of the 22 November 1977 earthquake at Willits, California: Activity in the Maacama fault zone, *Bull. Seismol. Soc. Am., 75*, 507–517, 1985.

Yerkes, R. F., and R. O. Castle, Seismicity and faulting attributable to fluid extraction, *Eng. Geol., 10*, 151–167, 1976.

Zoback, M. L., and M. D. Zoback, State of stress in the conterminous United States, *J. Geophys. Res., 85*, 6113–6156, 1980.

D. H. Oppenheimer, U.S. Geological Survey, 345 Middlefield Road, MS/977, Menlo Park, CA 94025.

(Received February 4, 1986;
revised June 13, 1986;
accepted July 7, 1986.)